

# Effect of Halogen Substitutions on dUMP to Stability of Thymidylate Synthase/dUMP/mTHF Ternary Complex Using Molecular Dynamics Simulation

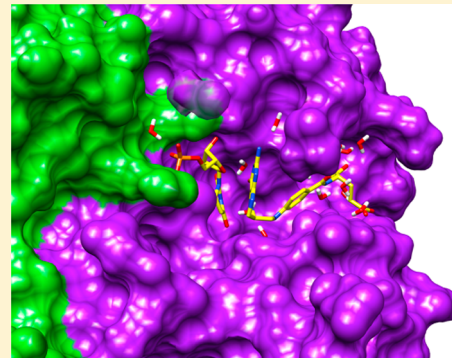
Nopporn Kaiyawet,<sup>†</sup> Thanyada Rungrotmongkol,<sup>‡</sup> and Supot Hannongbua<sup>\*,†</sup>

<sup>†</sup>Computational Chemistry Unit Cell, Department of Chemistry, Faculty of Science, Chulalongkorn University, 254 Phayathai Road, Patumwan, Bangkok 10330, Thailand

<sup>‡</sup>Department of Biochemistry, Faculty of Science, Chulalongkorn University, 254 Phayathai Road, Bangkok 10330, Thailand

## S Supporting Information

**ABSTRACT:** The stability of the thymidylate synthase (TS)/2-deoxyuridine-5-monophosphate (dUMP)/5,10-methylene-5,6,7,8-tetrahydrofolate (mTHF) ternary complex formation and Michael addition are considered as important steps that are involved in the inhibition mechanism of the anticancer prodrug 5-fluorouracil (5-FU). Here, the effect of three different halogen substitutions on the C-5 position of the dUMP (XdUMPs = FdUMP, CldUMP, and BrdUMP), the normal substrate, on the stability of the TS/dUMP and TS/dUMP/mTHF binary and ternary complexes, respectively, was investigated via molecular dynamics simulation. The simulated results revealed that the stability of all the systems was substantially increased by mTHF binding to the catalytic pocket. In the ternary complex, a much greater stabilization of the dUMP and XdUMPs through electrostatic interactions, including charge–charge and hydrogen bond interactions, was found compared to mTHF. An additional unique hydrogen bond between the substituted fluorine of FdUMP and the hydroxyl group of the TS Y94 residue was observed in both the binary and ternary complexes. The distance between the S<sup>−</sup> atom of the TS C146 residue and the C6 atom of dUMP, at <4 Å in all systems, suggested that a Michael addition with the formation of a S–C6 covalent bond potentially occurred, although the hydrogen atom on C6 of dUMP is substituted by a halogen atom. The MM/PBSA binding free energy revealed the significant role of the bridging waters around the ligands in the increased binding affinity (~10 kcal/mol) of dUMP/XdUMP, either alone or together with mTHF, toward TS. The order of the averaged binding affinity in the ternary systems was found to be CldUMP ≈ FdUMP > dUMP > BrdUMP, suggesting that CldUMP could be a potent candidate TS inhibitor, the same as FdUMP (the metabolite form of 5-FU).



## INTRODUCTION

Thymidylate synthase<sup>1</sup> (TS) is an enzyme that catalyzes the reductive methylation of 2-deoxyuridine-5-monophosphate (dUMP) to produce 2-deoxythymidine-5-monophosphate (dTDP) using the 5,10-methylene-5,6,7,8-tetrahydrofolate (mTHF) cofactor.<sup>2–6</sup> This folate cofactor not only acts as the carbon donor, but it also serves as a reducing agent.<sup>5,6</sup> Although the overall catalyzed reaction is presented as that of reductive methylation, the molecular mechanism of this reaction can be separately considered as a multistep reaction mechanism<sup>3</sup> (Figure 1).

The substrate binding into the TS active site is known to occur in an ordered fashion, forming the TS/dUMP binary complex and then the TS/dUMP/mTHF ternary complex, respectively,<sup>7</sup> where the configuration of the mTHF cofactor is substantially adjusted and activated simultaneously with the conformational change in the TS binding domain. Interestingly, mTHF binding into the active site involves several intrinsic steps which occur concomitantly and include the noncovalent ternary complex association, enzyme active site conformational

closure and mTHF conformational activation.<sup>4,8,9</sup> The nucleophilic attack (Michael addition) by the reactive cysteine residue of TS (C146) at the C-6 position of dUMP occurs simultaneously with the tight binding of the mTHF cofactor into the TS active site. Afterward, the C-5 position of dUMP is activated during the ongoing Michael addition that consequently leads to the ternary covalent complex formation between dUMP and the mTHF cofactor (intermediate V, Figure 1).<sup>10</sup> This step is followed by a β-elimination reaction, in which the Y94 residue of TS is proposed to act as a base and abstract the C-5 proton of dUMP<sup>11</sup> (intermediate VI, Figure 1) to generate exocyclic methylene (intermediate VII, Figure 1). Finally, this intermediate is reduced by the transfer of hydride from the H4-folate to produce dTMP and H2-folate.<sup>12</sup> This description is widely agreed as being the main mechanistic route of the overall reaction. However, some of the minor details are still open for discussion.

Received: March 1, 2013



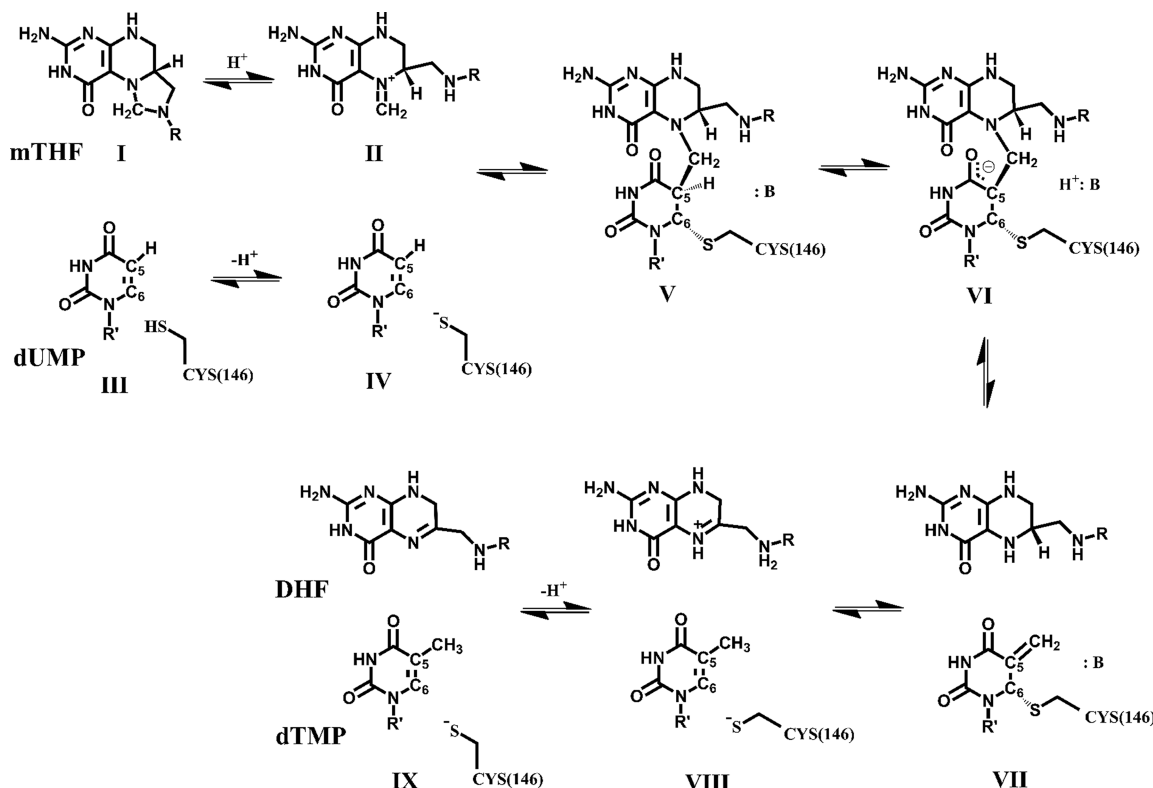


Figure 1. Multistep reductive methylation mechanism for thymidylate synthase (TS), as proposed by Carreras and Santi<sup>3</sup>.

5-Fluoro-dUMP (FdUMP), the metabolite form of the anticancer drug 5-fluorouracil (5-FU),<sup>13</sup> is an example of a successful dUMP analogue, which coreacts and forms a ternary covalent complex intermediate with the mTHF cofactor in a similar way as the native dUMP substrate.<sup>7,9</sup> However, the new C–F bonding requires a greater dissociation energy than the native C–H bonding and so leads to the termination of the  $\beta$ -elimination reaction in the TS/FdUMP/mTHF ternary complex.<sup>9</sup> Therefore, the FdUMP molecule likely remains trapped in the covalent intermediate form inside the TS active site leading to the irreversible loss of enzyme function. The fluorine substituent not only interferes with the  $\beta$ -elimination reaction but also directly influences the atomic charge of the C–S atom as well. This atomic charge change has been proposed to then influence the reactivity of the Michael addition reaction, which in turn indirectly effects the subsequent ternary covalent complex formation.<sup>14</sup>

The ternary covalent intermediate formation is achieved via many simultaneous steps of conformational activation of the two substrates, dUMP, and mTHF. The description of the effect of C-5 substituents on the ternary covalent complex formation without any interference from the other intrinsic reactions has so far been limited to that derived from experimental approaches. Molecular dynamics (MD) simulations were applied to investigate the dynamic properties as well as the intermolecular interaction between TS and the different dUMP halogen analogues using the TS/dUMP binary complex as the representative model.<sup>14</sup> Afterward, superimposition of the simulated binary complex to the crystal structure (static ternary complex structure) was used to broadly describe the effect of each halogen substituent on the ternary dynamics.

It is important to note here that there are two important reasons why the binary complex may not be assumed to reasonably describe or reflect the actual ternary complex behavior. First, the folate cofactor binding can shift the equilibrium constant of the Michael addition reaction to be favorable due to the presence of the thiol linkage intermediate instead of the free thiolate species.<sup>15</sup> Second, the flexibility of the enzyme catalytic domain is likely to lead to a different conformation between the presence (ternary complex) and absence (binary complex) of mTHF inside the TS binding pocket. Therefore, MD simulations using the binary complex model to investigate the stability and possibility of ternary complex formation according to the halogen substituents on the C-5 position of dUMP may still be questioned.

Here, we investigated the effect of halogen substitutions on the C-5 position of dUMP in the TS complex without and with mTHF (binary and ternary complexes, respectively) by means of a MD simulation approach. The results from this study could describe the importance of mTHF and the effect of halogen substitutions to noncovalent ternary complex formation prior to Michael addition in the TS enzyme.

## MATERIALS AND METHODS

**System Preparation.** To prepare the noncovalent ternary complex of either the dUMP substrate or its halogen analogues, the crystal structure of the TS/dUMP/THF complex (Figure 2), obtained from the Protein Data Bank (PDB code 1KZI),<sup>16</sup> was selected as the starting structure. The THF crystal structure was modified to be mTHF by the appropriate single group methylene addition, while the three XdUMP ligands (FdUMP, Cl<sub>2</sub>dUMP, and BrdUMP) were modeled by single atomic replacement on the C-5 hydrogen of dUMP with fluorine, chlorine, and bromine atoms, respectively. Meanwhile, the

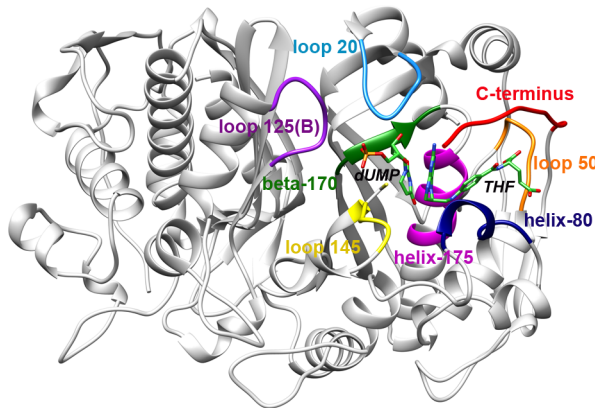


**Figure 2.** Crystal structure of the TS/dUMP/THF ternary complex (1KZI),<sup>16</sup> with the protein fragments important for the binding of dUMP and THF (stick model) shown in different colors.

mTHF structure in each ternary complex was removed to generate the relative binary complex.

**MD Simulation Details.** All ionizable amino acids were ionization state assigned at pH 7.0 using the PROPKA prediction software.<sup>17,18</sup> Missing hydrogen atoms were added using the LEaP module as implemented in the AMBER10 software package.<sup>19</sup> To obtain the partial atomic charges of mTHF, dUMP, and its analogues, quantum mechanics optimization in Gaussian03<sup>20</sup> with the HF/6-31G(d) basis set was performed for position refinement of all added hydrogen atoms and ESP charge calculation. The obtained charges were then converted to RESP charges using Antechamber in AMBER10 (the details of chemical structure scheme, atom types, and their partial charges shown in Figure S1 and Table S1 in Supporting Information). The systems were solvated with TIP3P water molecules<sup>21</sup> from 10 Å of protein surface ( $\sim$ 1500 molecules) in three dimensions ( $97 \times 81 \times 84$  Å) and 24 sodium ions were subsequently added in the system to achieve electrical charge neutralization. The periodic boundary condition was set with the isobaric-isothermal (NPT) ensemble under 1 atm of pressure, 310 K and with a Berendsen coupling time of 0.2 ps. The nonbonded interaction calculation was truncated within a 12 Å residue-base cutoff. The Particle Mesh Ewald method<sup>22</sup> was applied to account for long-range electrostatic interactions. The ff03 force-field and GAFF were used for parametrization of the protein and ligands, respectively. All of the covalent bonding involving the hydrogen atoms was constrained by a 2 fs step size with the SHAKE algorithm<sup>23</sup> during the simulations.

All water molecules were relaxed with 2000 steps of steepest descent (SD) and conjugated gradient (CG) minimization methods, whereas the protein and ligand coordinates were fixed. Afterward, all restrained forces were removed and the whole system was fully minimized by 2000 steps of SD and CG. The system was heated up to 310 K over 200-ps simulation and pre-equilibrated for 300 ps with the position of the two ligands and bridging water molecules inside the protein binding pocket restrained with 50 kcal/mol·Å<sup>2</sup> factors to maintain their positions. The restrained force on the two ligands were then reduced to 30, 20, 10, 5, 2, and 0 kcal/mol·Å<sup>2</sup> every 250 ps, while that for the bridging water molecules was correspondingly reduced to 30, 30, 20, 10, 5, and 2 kcal/mol·Å<sup>2</sup>. Afterward, all atoms were allowed to move freely without any restrained force for 20 ns of simulation time.

**MM/PBSA and MM/GBSA Methods.** The 100 MD snapshots extracted from the last 10 ns of each system were used as the structural ensemble in an estimated binding free energy calculation considered by free energy difference between protein–ligand complex and the individual forms

$$\Delta G_{\text{binding}} = G_{\text{complex}} - [G_{\text{protein}} + G_{\text{ligand}}] \quad (1)$$

where  $G_{\text{complex}}$ ,  $G_{\text{protein}}$ , and  $G_{\text{ligand}}$  refer to the absolute free energy of the complex, protein, and ligands, respectively. The binding free energy is composed of the molecular mechanics energy ( $\Delta E_{\text{MM}}$ ), entropy ( $\Delta S$ ), and solvation free energy ( $\Delta G_{\text{sol}}$ ) as given in eq 2.

$$\Delta G_{\text{binding}} = \Delta E_{\text{MM}} - T\Delta S + \Delta G_{\text{sol}} \quad (2)$$

The  $\Delta E_{\text{MM}}$  is obtained by a combination of electrostatic ( $\Delta E^{\text{ele}}$ ) and van der Waals ( $\Delta E^{\text{vdW}}$ ) interaction energies. The  $T\Delta S$  term represents the solute entropic contribution at temperature  $T$  (Kelvin). In this study, this term is approximated by very small entropic difference due to the mimic structure of dUMP and its three halogen analogues; therefore, the  $\Delta G_{\text{binding}}$  is predicted by excluding the entropy contribution. The  $\Delta G_{\text{sol}}$  is described from the electrostatic ( $\Delta G_{\text{sol}}^{\text{ele}}$ ) and nonpolar ( $\Delta G_{\text{sol}}^{\text{nonpolar}}$ ) free energies of solvation as

$$\Delta G_{\text{sol}} = \Delta G_{\text{sol}}^{\text{ele}} + \Delta G_{\text{sol}}^{\text{nonpolar}} \quad (3)$$

The  $\Delta G_{\text{sol}}^{\text{ele}}$  can be approximately calculated by Poisson–Boltzmann (PB) or Generalized-Born (GB) models. The Poisson–Boltzmann formula<sup>24–26</sup> is summarized as follows:

$$\nabla \cdot (\epsilon(r) \nabla \cdot \phi(r)) - \kappa(r)^2 \epsilon(r) \sinh[\phi(r)] \\ = -4\pi\rho^f(r)/k_B T \quad (4.1)$$

$$\kappa^2(r) = \frac{8\pi q^2 I}{ek_B T} \quad (4.2)$$

where  $\phi(r)$ ,  $T$ ,  $q$ ,  $\epsilon$ , and  $\rho^f$  refer the dimensionless electrostatic potential, absolute temperature, atomic number, dielectric constant and the fixed charge density (in proton charge units), respectively. The  $\kappa^2$  is the Debye–Hückel parameter, and  $I$  is the ionic strength of the solution. Alternatively, the  $\Delta G_{\text{sol}}^{\text{ele}}$  can also be accounted by the Generalized Born (GB) model<sup>27,28</sup> as defined in eq 5.1 and 5.2.

$$\Delta G_{\text{sol}}^{\text{ele}} = -\frac{1}{2} \left(1 - \frac{1}{\epsilon}\right) \sum_{k,k'} q_k q_{k'} \gamma_{kk'} \quad (5.1)$$

$$\gamma_{kk'} = \left( R_{kk'} + \alpha_k \alpha_{k'} \left( \exp\left(\frac{-r_{kk'}^2}{d_{kk} \alpha_k \alpha_{k'}}\right) + C_{kk'} \right) \right)^{-1/2} \quad (5.2)$$

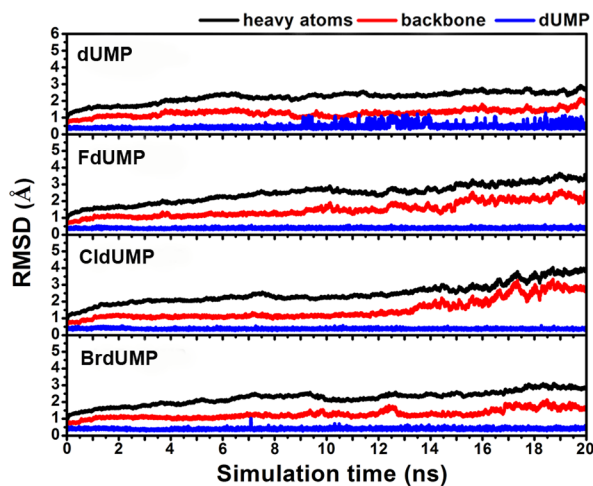
where  $q_k$ ,  $C_{kk'}$ ,  $R_{kk'}$ ,  $\alpha_k$  and  $d_{kk}$  are partial charge on atom  $k$ , Coulomb integral, inter atomic distance, effective atomic radius and an empirically optimized constant, respectively. In contrast, the  $\Delta G_{\text{sol}}^{\text{nonpolar}}$  is gained by evaluating the solvent accessible surface area (SASA)<sup>29</sup>

$$\Delta G_{\text{sol}}^{\text{nonpolar}} = \gamma \text{SASA} + b \quad (8)$$

where the  $\gamma$  and  $b$  represent the experimental solvation parameters equal to 0.00542 kcal/mol·Å<sup>2</sup> and 0.92 kcal/mol,<sup>29</sup> respectively.

The free energy calculation is also used to evaluate per-residue decomposition (DC) toward ligand binding. Because of

## (A) Binary complex



## (B) Ternary complex

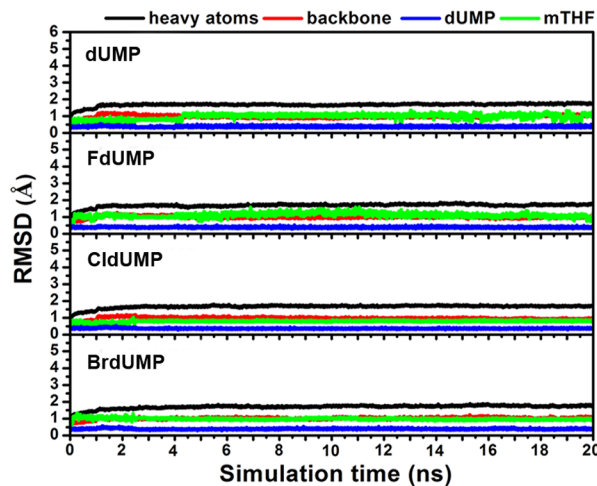
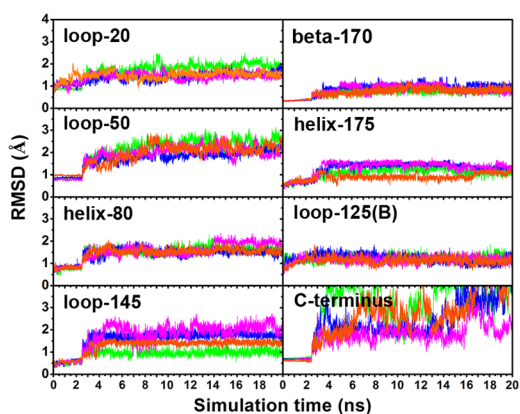
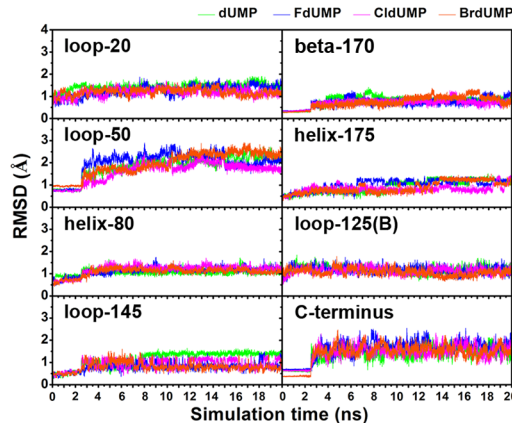


**Figure 3.** RMSD plot for all heavy atoms and the protein backbone of TS and ligand heavy atoms versus simulation time of the (A) binary complexes and (B) ternary complexes relative to the starting structure.

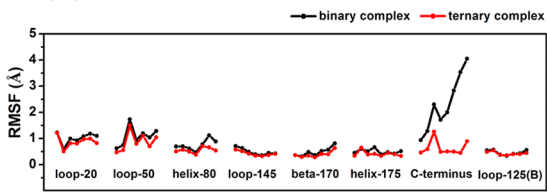
## (A) Binary complex



## (B) Ternary complex



## (C)



## (D)

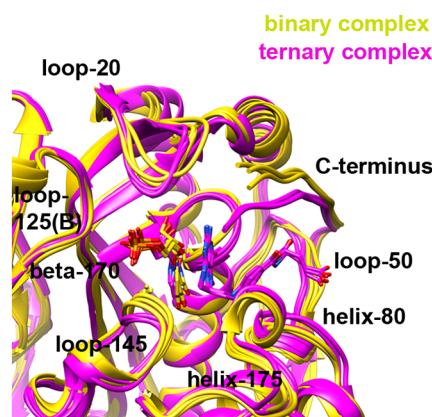


**Figure 4.** RMSD versus simulation time of each binding domain fragment compared between the (A) absence (binary complex) and (B) presence (ternary complex) of the mTHF cofactor inside the TS binding pocket. (C) RMSF of the binding pocket fragments during the last 10 ns for the dUMP binary and ternary complexes where their MD trajectories at nearly end of each simulation are superimposed in (D).

faster calculation in MM/GBSA procedure, it becomes more attractive than MM/PBSA.<sup>30</sup> By following the concept of free energy difference between any two considered states (bounded and unbounded forms), the perturbation pathway with free energy perturbation (FEP) formalism can also be applied to

evaluate the local stabilization free energy contribution of each residue to ligand binding comparatively.<sup>31,32</sup> Moreover, these methods are also used to investigate free energy change because of the substituent effect or artificial mutagenesis (from any residue to glycine or alanine, for example).<sup>33,34</sup>

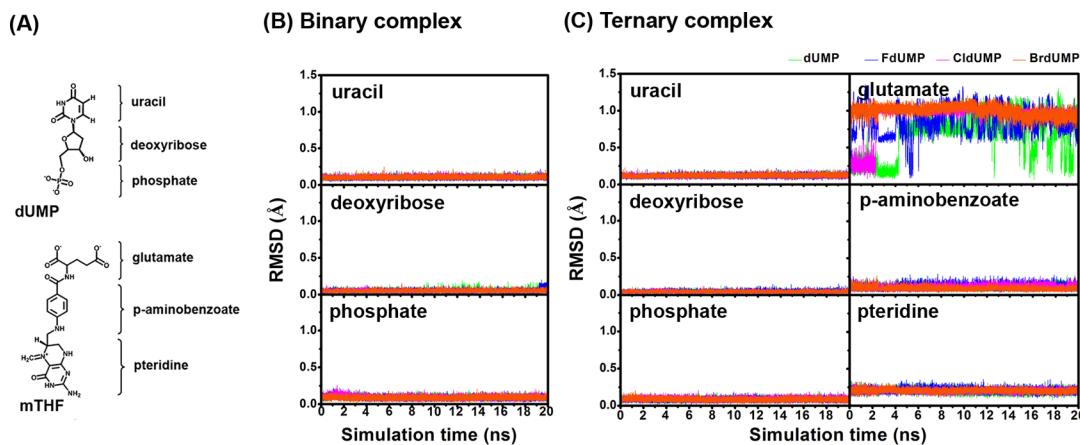


**Figure 5.** (A) Chemical structure of dUMP and mTHF. Dynamic flexibility of the different dUMP and mTHF fragments, as evaluated by means of RMSD calculation in the (B) binary and (C) ternary complexes.

## RESULTS AND DISCUSSION

**Overall Enzyme and Substrates Stability.** To monitor the stability of each simulated system, the root-mean-square displacements (RMSD) along the simulation time of all heavy atoms, protein backbone atoms and ligand heavy atoms was measured and then plotted in Figure 3. The RMSD of all the heavy atoms and backbone atoms in the binary complexes (Figure 3A) revealed a slightly increased curve in a range of 1.0–2.5 Å during the first 12 ns in all four evaluated systems. After the 14 ns, the plots tended to fluctuate over an extended range, especially for the FdUMP and CldUMP complexes. This is in contrast to that observed for all the ternary complexes (Figure 3B), where these plots fluctuated much less and the systems reached equilibrium after 1 ns. Meanwhile, the plots of dUMP and its analogues in both the binary and ternary complexes revealed a very narrow fluctuation range of less than 1.0 Å till the end of the simulation. The low fluctuation level observed for mTHF was similar to that for dUMP (only 0.5 Å higher RMSD values). Thus, the inclusion of mTHF into the TS binding site to form the ternary complex led to a noticeable increase in the protein stability. Accordingly, the dynamic property of TS in the absence of the mTHF cofactor (binary complex) may not be assumed to reasonably describe the ternary complex behavior, in contrast to a previous study.<sup>14</sup>

The important fragments (five flexible loops, two helices and a  $\beta$  sheet) involved in the binding sites for dUMP and mTHF are shown in Figure 2. To explore the effect of mTHF binding on the TS active site conformation, which may involve a change in the overall protein flexibility, the fluctuation in the conformation of these fragments was considered in terms of comparing the respective regions of the RMSD plots between the binary and ternary complexes (Figure 4A and 4B). Additionally, their root-mean-square fluctuations (RMSFs) in the two dUMP systems (for example) from the last 10-ns simulation were compared in Figure 4C where the superimposed structures were depicted in Figure 4D.

The RMSD profiles can classified into three broadly different patterns, depending on the magnitude of the fluctuation, as low (0–1.5 Å), medium (1.5–2.5 Å) and high (>2.5 Å) flexibilities. Noticeably, the fluctuation of the C-terminal fragment was found to have a relatively high flexibility along the fully unrestrained simulation times for all binary complexes, while it displayed only a medium flexibility in the ternary complex instead. From the X-ray structure of the TS/dUMP/THF

ternary complex (Figure 2), the C-terminus is not only specified as the binding gateway to support the incoming substrates but to also play an important role in stabilizing the folate cofactor during the ternary complex formation. Therefore, the presence of the mTHF cofactor in the binding pocket reduces the flexibility of C-terminal fragment significantly. The loop-20, helix-80 and loop-145 domains showed a medium flexibility in the binary complex but were more rigid in the ternary complex, whereas the level of fluctuation of the rest of the fragments (loop-50, beta-170, helix-175 and loop-125(B)) was similar between the two complexes. Since in all the systems, including the ligand binding fragments (Figures 3 and 4), equilibrium was reached at 10 ns, their MD trajectories from the last 10 ns were collected for intermolecular interaction and binding free energy analysis. The RMSF plots of the binding pocket fragments for the dUMP systems (as an example, Figure 4C) and their superimposed MD structures in Figure 4D well supported the RMSD results.

dUMP is comprised of the three main components of a uracil base, deoxyribose, and phosphate groups, while mTHF is comprised of pteridine, p-aminobenzoate (PABA), and glutamate groups (Figure 5A). The RMSD of their heavy atoms in the binary and ternary complexes were plotted to evaluate their conformational flexibility and are compared in Figure 5B and 5C, respectively. All three dUMP components showed a very low magnitude of fluctuation with or without mTHF cofactor binding. For mTHF in the ternary complex, a high conformational flexibility was principally found in the glutamate component while the pteridine and PABA groups remained fairly rigid and in the range with those of dUMP. This indicates that the higher structural flexibility of mTHF (Figure 3B) is mostly located on the glutamate portion that is positioned on the surface of TS and fully solvated by water (Figure 2). Interestingly, the very high flexibility of the glutamate group of mTHF had no influence on the pteridine and PABA conformations of the same molecule. Taken together, dUMP occupies the inside of the binding pocket rigidly in both the binary and ternary complexes (absence and presence of mTHF, respectively), while the reactive pteridine group of mTHF that is involved in the methylene bridging formation after Michael addition is unlikely to be affected by the flexibility of the glutamate component at the other end of the molecule.

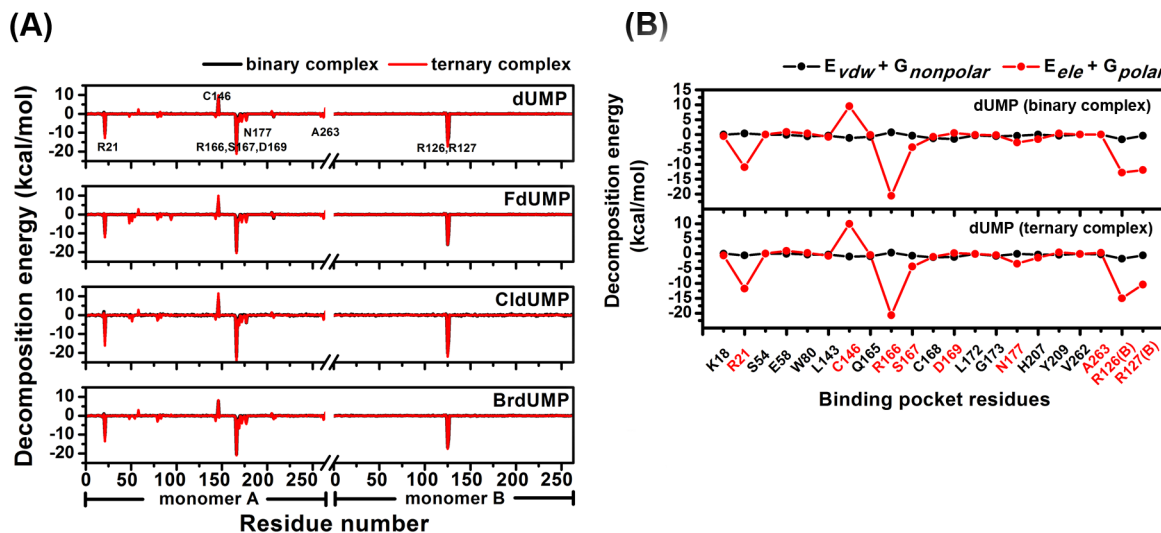


**Figure 6.** (A) Decomposition binding free energy scanning in pairwise per-residue basis of all TS residues for the binding of dUMP and the three XdUMPs derivatives in the binary and ternary complexes. (B) The energy components, electrostatic ( $E_{ele} + G_{polar}$ ) and van der Waals ( $E_{vdw} + G_{nonpolar}$ ) terms, for the nine key residues of dUMP in the binary and ternary complex.

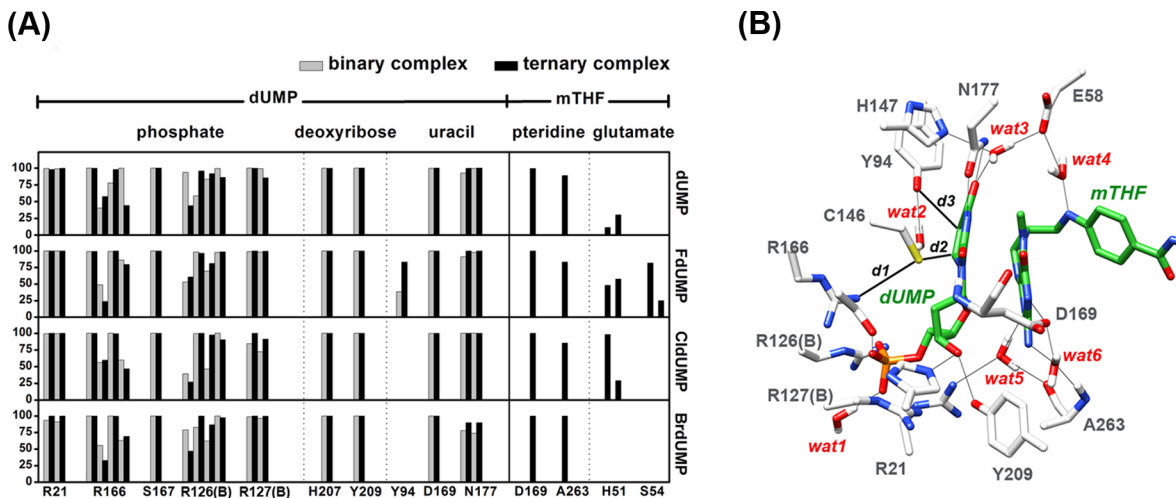


**Figure 7.** (A) Percentage occupation of hydrogen bonding for dUMP (or XdUMP analogues) and mTHF binding to the TS residues in the binary (light gray) and ternary (black) complexes. (B) Close up of dUMP and mTHF (green) in the TS catalytic pocket where the dashed and solid lines represent the hydrogen bonding and the intermolecular distances,  $d_1$ – $d_3$ , involved in the active conformation and in the Michael addition, respectively.

**Per-Residue Decomposition Energy Scanning.** To scan the important residues for ligand binding, the per-residue energy contribution was calculated from the MM-GBSA decomposition (DC) energy. The DC energies of all protein residues for ligand binding between the binary and ternary complexes are shown in Figure S2 (Supporting Information). Most of the energy stabilization was found for dUMP binding while no stabilization was detected for mTHF. Therefore, only dUMP (as well as its analogues) was analyzed further (Figure 6A).

The overall per-residue energy pattern for dUMP and XdUMP analogs was found to be similar in both the binary and ternary complexes (Figure 6A), where the main stabilization was contributed from the four arginine residues (R21, R166, R126(B), and R127(B)) at  $< -10$  kcal/mol, and also to a lesser extent from the S167, D169, N177 and A263 residues at  $\sim -5$  kcal/mol. In contrast, the reactive C146 residue of TS provided a destabilization energy of about  $\sim 10$  kcal/mol in the negatively

charged state due to the strong repulsive interaction with the phosphate group of dUMP and its analogues. The DC energy of these nine important residues toward the binding of dUMP, as a representative ligand, was considered in terms of electrostatic and van der Waals energies including the solvation effect (Figure 6B). From the plots it appears that dUMP mainly bound to TS through electrostatic interactions, while the contribution from van der Waals interactions was rather weak.

**Enzyme–Substrates interactions.** Because the electrostatic interaction was found to be important in dUMP binding and hydrogen bonding is basically an electrostatic interaction, then the hydrogen bonding formation between dUMP (and mTHF) with the TS residues was evaluated. To this end, the percentage of hydrogen bonding occupation was monitored using the two acceptance criteria of (i) a distance between the proton donor (D) and acceptor (A) atoms of  $\leq 3.5$  Å and (ii) an angle of  $D-H\cdots A > 120^\circ$ . The obtained results for all the binary and ternary systems are plotted in Figure 7A, while the

hydrogen bonding pairs are represented by dashed lines in Figure 7B. Comparison of the data for dUMP and mTHF in the ternary complexes revealed that the likely number of hydrogen bonds formed was substantially higher for dUMP (at least 18 hydrogen bonds involving 10 residues) than for mTHF (four hydrogen bonds). The hydrogen bonding patterns found for dUMP were similar in both the binary and ternary systems and so correspond with the DC results. The main stabilization was found at its phosphate moiety, according to the strong salt-bridge interaction with the four surrounded arginines (R21, R166, R126(B), and R127(B)) and a serine S167. In addition, a lower hydrogen bond occupation level was found in the deoxyribose (H207 and Y209) and uracil (D169 and N177) moieties. Interestingly, an additional H-bond was formed between the substituted fluorine of FdUMP and the Y94 residue of TS, and this was considerably stronger by in ternary complex (80% occupancy) than in the binary complex (40% occupancy).

With respect to mTHF, among the three fragments (pteridine, PABA, and glutamate), no hydrogen bonding was found at PABA, which is because of its nonpolar aromatic ring. The pteridine groups makes two strong hydrogen bonding interactions with the D169 and A263 residues of TS. Note that the TS D169 residue forms a strong hydrogen bonding with both dUMP and mTHF (nearly 100% occupancy) leading to the conformational trapping in a  $\pi-\pi$  stacking between the uracil of dUMP and the pteridine of mTHF. The significance of this residue is supported by the deficiency of the ternary complex formation in the mutated TS of *Lactobacillus casei* (D221 numbering in *L. casei*).<sup>35</sup> The terminal glutamate of mTHF, which is positioned on the protein surface, was found to be partially stabilized by two residues: H51 in all ternary systems except for BrdUMP, and S54 only in FdUMP.

**Reaction Coordinate Distance Analysis.** The substitution on the C5 position of dUMP with electron withdrawing groups was previously proposed in a QSAR study to increase the reactivity of the Michael addition reaction in TS.<sup>14</sup> To investigate the effect of halogen substitutions at this position on the active conformation of the binary and ternary complexes in the Michael addition, the distribution of the three intermolecular distances of (i)  $d_1[S(C146)-NH2(R166)]$  between the reactive C146 and the stabilized R166, (ii)  $d_2[S(C146)-C6(dUMP)]$  responsible for the focused reaction, and (iii)  $d_3[O(Y94)-C5(dUMP)]$  that corresponds to a unique hydrogen bond with the TS Y94 residue, was monitored (see Figure 7B for the definition of  $d_1-d_3$ ) and is plotted in Figure 8.

Prior to the Michael addition, the reactive TS C146 residue was activated by R166<sup>36</sup>, while this arginine residue plays a role in stabilizing the negative charge of C146 via the strong charge–charge interaction. This is well supported by the narrow and sharp peak of  $d_1$  at  $\sim 3.2 \text{ \AA}$  observed in all systems. From the  $d_2$  plot, which is directly involved in the Michael addition, the most probable finding for  $d_2$  in all ternary complexes was within the range of  $2.7-3.7 \text{ \AA}$  (solid lines), whereas the absence of mTHF in the binary complex leads to more movement of dUMP with a slight shift in  $d_2$  to  $4.0 \text{ \AA}$  (dashed lines). The similar range of  $d_2$  values found in all systems suggests the Michael addition on the C-6 position of the dUMP analogue is possible but may differ in the activation energy of the reaction depending on the nature of the chemical structure. In addition, the unique hydrogen bonding interaction between the substituted fluorine and the TS Y94 hydroxyl group in the FdUMP system is confirmed by the shortening of

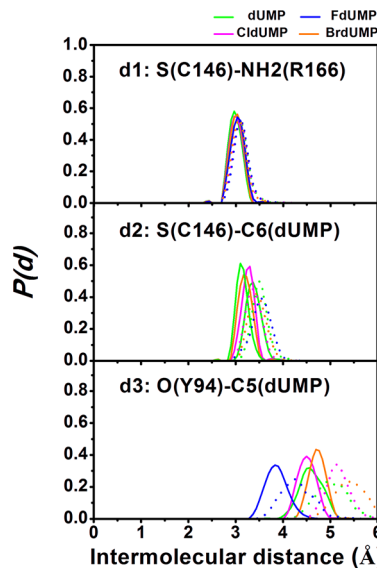


**Figure 8.** Distribution plot of the  $d_1-d_3$  intermolecular distances,  $P(d)$ , sampling from the last 10-ns simulation in the binary (dashed line) and ternary (solid line) complexes.

the related  $d_3$  distance (blue). Therefore, this substitution on the C-5 position of dUMP that can form a strong hydrogen bond with the Y94 residue may lead to an increased ligand binding affinity with the TS target.

**Ligand Binding Affinity.** The MM/PBSA module implemented in AMBER was used to evaluate the binding strength of the individual dUMP/XdUMP substrates and both the mTHF cofactor and dUMP/XdUMP substrates with TS in the binary and ternary systems, respectively, with the results being given in Table 1. The X-ray structure of the TS/dUMP/THF ternary complex<sup>16</sup> revealed three water molecules bridged between each ligand and TS residues, which may feasibly facilitate the orientation of ligands to be correctly located in the binding pocket. The characteristic behaviors of the bridged waters including degree of freedom (vibration, translation and rotation modes)<sup>37,38</sup> apparently differ from the general bulk waters, therefore, these waters must be carefully considered. From this concern, the free energy of ligand binding to TS embedded with or without the bridging waters was calculated, and the results are compared Table 1. Note that the alternative methods for prediction of binding free energy for ligand-protein complex and determination of the water bridging network important for structural stabilization are linear interaction energy (LIE)<sup>39,40</sup> and linear response approximation (LRA)<sup>41,42</sup> for example.

From Table 1, the inclusion of bridging waters was found to increase the binding free energy of the ligands by  $>10 \text{ kcal/mol}$  in all binary and ternary complexes, suggesting the important role of bridging waters in the stabilization of ligand binding. Based on the predicted binding free energies (kcal/mol), the order of binding affinity for the ternary systems was (highest to lowest): CldUMP ( $-100.3$ )  $\approx$  FdUMP ( $-96.8$ )  $>$  dUMP ( $-86.3$ )  $>$  BrdUMP ( $-77.8$ ). Interestingly, the binding free energy order observed in the binary complexes are a little different (dUMP  $\approx$  FdUMP  $\approx$  CldUMP  $>$  BrdUMP) with reduced energies relative to those of the ternary complexes. Moreover, dUMP or its analogues binds to TS some 3-fold stronger than mTHF, in accord with the results for the per-residue DC free energy and hydrogen bonding interactions.

**Table 1.** Averaged Binding Free Energy (kcal/mol), over 100 Snapshots Taken from the Last 10 ns of MD Simulation, of the Ligands Binding to TS Enzyme in the Binary and Ternary Complexes, with the Standard Deviation Shown in Brackets

receptor	ligand	binary complex				ternary complex			
		dUMP	FdUMP	CldUMP	BrdUMP	dUMP	FdUMP	CldUMP	BrdUMP
TS	dUMP <sup>a</sup> and mTHF					-71.9 (10.3)	-77.8 (8.9)	-82.8 (11.1)	-65.4 (6.7)
TS and wat1–6	dUMP <sup>a</sup> and mTHF					-86.3 (11.0)	-96.8 (9.6)	-100.3 (10.7)	-77.8 (11.9)
TS	dUMP <sup>a</sup>	-59.5 (6.6)	-59.1 (7.4)	-59.8 (7.5)	-53.0 (8.8)	-76.4 (11.2)	-87.1 (9.4)	-88.6 (11.7)	-69.9 (10.8)
TS	mTHF					-19.8 (6.1)	-28.1 (5.2)	-26.7 (5.4)	-22.3 (6.3)
TS and wat1–3	dUMP <sup>a</sup>	-70.9 (6.7)	-72.5 (8.3)	-70.3 (10.1)	-55.5 (8.7)				

<sup>a</sup>dUMP or XdUMPs.

## CONCLUSION

In the present study, the effect of halogen substitutions on the C-5 position of dUMP toward the stability of the binary and ternary complexes was investigated by means of MD simulations. From the simulated results, the stability of the system and the ligand binding fragments were found to be significantly increased, and in particular for the C-terminal region of TS, in the ternary complexes. The dUMP and its halogen analogues were principally stabilized through electrostatic interactions including charge–charge and hydrogen bond interactions, whereas no direct stabilization was found for the binding of the mTHF cofactor. In both the binary and ternary complexes, a strong hydrogen bond formation was found between the phosphate moiety of dUMP/XdUMP and the four surrounding TS arginines residues (R21, R166, R126(B), and R127(B)). Interestingly, a unique hydrogen bond between the substituted fluorine on dUMP and the TS Y94 hydroxyl group was observed with FdUMP in both the binary and ternary complexes, supporting the effective inhibitory activity of FdUMP, the metabolite form of the anticancer prodrug 5-FU. The distance between the S<sup>−</sup> atom of the reactive C146 residue of TS and the C6 atom of dUMP, involved in the Michael addition, was decreased from 4.0 Å in the binary complexes to 2.7–3.7 Å in the ternary complexes, suggesting that the Michael addition on the C-6 position of the dUMP is possible and proceeded in all of the C-5 halogen analogues substitutions. Based on the MM/PBSA method, the bridging waters were shown to have a significant role in increasing the binding affinity of dUMP/XdUMP, alone or together with mTHF, toward TS with a lowered binding free energy of 10 kcal/mol. The dUMP (or its analogues) showed a 3-fold stronger binding to TS than did mTHF, and the order of their averaged binding affinity was CldUMP ≈ FdUMP > dUMP > BrdUMP in the ternary systems, suggesting that the CldUMP may serve as a potent candidate for TS inhibition.

## ASSOCIATED CONTENT

### Supporting Information

Chemical structures of mTHF and dUMP and its analogues, decomposition energy on a pairwise per-residue basis for all the TS residues in the binding of dUMP and mTHF in the binary and ternary complexes, atom names, atom types, and partial atomic charges (*q*) of mTHF and dUMP and its analogue. This material is available free of charge via the Internet at <http://pubs.acs.org>.

## AUTHOR INFORMATION

### Corresponding Author

\*Fax: +662-218-7603. Tel: +662-218-7603. E-mail: supot.h@chula.ac.th.

### Notes

The authors declare no competing financial interest.

## ACKNOWLEDGMENTS

This work was supported by the Asahi Glass Foundation, and Chulalongkorn University. The Thai Government Stimulus Package 2 (TKK2555) under the Project for Establishment of Comprehensive Center for Innovative Food, Health Products and Agriculture is greatly acknowledged for computing resources. N.K. thanks the Royal Golden Jubilee Ph.D. Program (PHD/0322/2550) and T.R. thanks the grants for the development of new faculty staff (the Ratchadaphiseksomphot Endowment Fund). We also thank the Higher Education Research Promotion and National Research University Project of Thailand, Office of the Higher Education Commission (HR1155A).

## REFERENCES

- (1) Perry, K. M.; Fauman, E. B.; Finer-Moore, J. S.; Montfort, W. R.; Maley, G. F.; Maley, F.; Stroud, R. M. Plastic adaptation toward mutations in proteins: Structural comparison of thymidylate synthases. *Proteins: Struct., Funct., Bioinf.* **1990**, *8*, 315–333.
- (2) Stroud, R. M.; Finer-Moore, J. S. Stereochemistry of a multistep/bipartite methyl transfer reaction: thymidylate synthase. *FASEB J.* **1993**, *7*, 671–677.
- (3) Carreras, C. W.; Santi, D. V. the Catalytic Mechanism and Structure of Thymidylate Synthase. *Annu. Rev. Biochem.* **1995**, *64*, 721–762.
- (4) Spencer, H. T.; Villafranca, J. E.; Appleman, J. R. Kinetic scheme for thymidylate synthase from *Escherichia coli*: Determination from measurements of ligand binding, primary and secondary isotope effects, and pre-steady-state catalysis. *Biochemistry* **1997**, *36*, 4212–4222.
- (5) Santi, D. V. Perspective on the design and biochemical pharmacology of inhibitors of thymidylate synthetase. *J. Med. Chem.* **1980**, *23*, 103–111.
- (6) Danenberg, P. V. Thymidylate synthetase—A target enzyme in cancer chemotherapy. *Biochim. Biophys. Acta* **1977**, *473*, 73–92.
- (7) Santi, D. V.; Danenberg, P. V. In *Folates and Pterins*; Blackley, R. L., Benkovic, S. J., Eds.; John Wiley & Sons: New York: 1984; Vol. 1, pp 345–398.
- (8) Matthews, D. A.; Villafranca, J. E.; Janson, C. A.; Smith, W. W.; Welsh, K.; Freer, S. Stereochemical mechanism of action for thymidylate synthase based on the X-ray structure of the covalent inhibitory ternary complex with 5-fluoro-2'-deoxyuridylate and 5,10-methylenetetrahydrofolate. *J. Mol. Biol.* **1990**, *214*, 937–948.

- (9) Santi, D. V.; McHenry, C. S.; Raines, R. T.; Ivanetic, K. M. Kinetics and thermodynamics of the interaction of 5-fluoro-2'-deoxyuridylate with thymidylate synthase. *Biochemistry* **1987**, *26*, 8606–8613.
- (10) Barrett, J. E.; Maltby, D. A.; Santi, D. V.; Schultz, P. G. Trapping of the C5-methylene intermediate in thymidylate synthase. *J. Am. Chem. Soc.* **1998**, *120*, 449–450.
- (11) Liu, Y.; Barrett, J. E.; Schulz, P. G.; Santi, D. V. Tyrosine 146 of thymidylate synthase assists proton abstraction from the 5-position of 2'-deoxyuridine 5'-monophosphate. *Biochemistry* **1999**, *38*, 848–852.
- (12) Barrett, J. E.; Lucero, C. M.; Schultz, P. G. A model for hydride transfer in thymidylate synthase based on unnatural amino acid mutagenesis. *J. Am. Chem. Soc.* **1999**, *121*, 7965–7966.
- (13) Parker, W. B.; Cheng, Y. C. Metabolism and mechanism of action of 5-fluorouracil. *Pharmacol. Ther.* **1990**, *48*, 381–395.
- (14) Jarmula, A.; Cieplak, P.; Krygowski, T. M.; Rode, W. The effect of 5-substitution in the pyrimidine ring of dUMP on the interaction with thymidylate synthase: Molecular modeling and QSAR. *Bioorg. Med. Chem.* **2007**, *15*, 2346–2358.
- (15) Moore, M. A.; Ahmed, F.; Dunlap, R. B. Trapping and partial characterization of an adduct postulated to be the covalent catalytic ternary complex of thymidylate synthase. *Biochemistry* **1986**, *25*, 3311–3317.
- (16) Fritz, T. A.; Liu, L.; Finer-Moore, J. S.; Stroud, R. M. Tryptophan 80 and leucine 143 are critical for the hydride transfer step of thymidylate synthase by controlling active site access. *Biochemistry* **2002**, *41*, 7021–7029.
- (17) Li, H.; Robertson, A. D.; Jensen, J. H. Very fast empirical prediction and rationalization of protein pKa values. *Proteins: Struct., Funct., Bioinf.* **2005**, *61*, 704–721.
- (18) Bas, D. C.; Rogers, D. M.; Jensen, J. H. Very fast prediction and rationalization of pKa values for protein-ligand complexes. *Proteins: Struct., Funct., Bioinf.* **2008**, *73*, 765–783.
- (19) Case, D. A.; Darden, T. A.; Cheatham, T. E. I.; Simmerling, C. L.; Wang, J.; Duke, R. E.; Luo, R.; Crowley, W.; Walker, R. C.; Zhang, W.; Merz, K. M.; Wang, B.; Hayik, S.; Roitberg, A.; Seabra, G.; Kolossvary, I.; Wong, K. F.; Paesani, F.; Vanicek, J.; Wu, X.; Brozell, S. R.; Steinbrecher, T.; Gohlke, H.; Yang, L.; Tan, C.; Mongan, J.; Hornak, V.; Cui, G.; Mathews, D. H.; Seein, M. G.; Sagui, C.; Babin, V.; Kollman, P. A. AMBER 10; University of California: San Francisco, CA, 2008.
- (20) Frisch, M. J.; Trucks, G. W.; Schlegel, H. B.; Scuseria, G. E.; Robb, M. A.; Cheeseman, J. R.; Montgomery, J. A., Jr.; Vreven, T.; Kudin, K. N.; Burant, J. C.; Millam, J. M.; Iyengar, S. S.; Tomasi, J.; Barone, V.; Mennucci, B.; Cossi, M.; Scalmani, G.; Rega, N.; Petersson, G. A.; Nakatsuji, H.; Hada, M.; Ehara, M.; Toyota, K.; Fukuda, R.; Hasegawa, J.; Ishida, M.; Nakajima, T.; Honda, Y.; Kitao, O.; Nakai, H.; Klene, M.; Li, X.; Knox, J. E.; Hratchian, H. P.; Cross, J. B.; Bakken, V.; Adamo, C.; Jaramillo, J.; Gomperts, R.; Stratmann, R. E.; Yazyev, O.; Austin, A. J.; Cammi, R.; Pomelli, C.; Ochterski, J. W.; Ayala, P. Y.; Morokuma, K.; Voth, G. A.; Salvador, P.; Dannenberg, J. J.; Zakrzewski, V. G.; Dapprich, S.; Daniels, A. D.; Strain, M. C.; Farkas, O.; Malick, D. K.; Rabuck, A. D.; Raghavachari, K.; Foresman, J. B.; Ortiz, J. V.; Cui, Q.; Baboul, A. G.; Clifford, S.; Cioslowski, J.; Stefanov, B. B.; Liu, G.; Liashenko, A.; Piskorz, P.; Komaromi, I.; Martin, R. L.; Fox, D. J.; Keith, T.; Al-Laham, M. A.; Peng, C. Y.; Nanayakkara, A.; Challacombe, M.; Gill, P. M. W.; Johnson, B.; Chen, W.; Wong, M. W.; Gonzalez, C.; Pople, J. A. Gaussian 03, revision x.x; Gaussian, Inc.: Wallingford, CT, 2004.
- (21) Jorgensen, W.; Chandrasekhar, J.; Madura, J.; Impey, R.; Klein, M. Comparison of simple potential functions for simulating liquid water. *J. Chem. Phys.* **1983**, *79*, 926–935.
- (22) York, D. M.; Darden, T. A.; Pedersen, L. G. The effect of long-range electrostatic interactions in simulations of macromolecular crystals: A comparison of the Ewald and truncated list methods. *J. Chem. Phys.* **1993**, *99*, 8345–8348.
- (23) Ryckaert, J. P.; Ciccotti, G.; Berendsen, H. J. C. Numerical integration of the cartesian equations of motion of a system with constraints: Molecular dynamics of n-alkanes. *J. Comput. Phys.* **1977**, *23*, 327–341.
- (24) Honig, B.; Nicholls, A. Classical electrostatics in biology and chemistry. *Science* **1995**, *268*, 1144–1149.
- (25) Cai, Q.; Wang, J.; Zhao, H.-K.; Luo, R. On removal of charge singularity in Poisson–Boltzmann equation. *J. Chem. Phys.* **2009**, *130*, No. 145101.
- (26) Cai, Q.; Hsieh, M.-J.; Wang, J.; Luo, R. Performance of Nonlinear Finite-Difference Poisson–Boltzmann Solvers. *J. Chem. Theory Comput.* **2010**, *6*, 203–211.
- (27) Hawkins, G. D.; Cramer, C. J.; Truhlar, D. G. Parametrized models of aqueous free energies of solvation based on pairwise descreening of solute atomic charges from a dielectric medium. *J. Phys. Chem.* **1996**, *100*, 19824–19839.
- (28) Hawkins, G. D.; Cramer, C. J.; Truhlar, D. G. Pairwise solute descreening of solute charges from a dielectric medium. *Chem. Phys. Lett.* **1995**, *246*, 122–129.
- (29) Sitkoff, D.; Sharp, K. A.; Honig, B. Accurate calculation of hydration free energies using macroscopic solvent models. *J. Phys. Chem.* **1994**, *98*, 1978–1988.
- (30) Gohlke, H.; Kiel, C.; Case, D. A. Insights into protein–protein binding by binding free energy calculation and free energy decomposition for the Ras–Raf and Ras–RalGDS complexes. *J. Mol. Biol.* **2003**, *330*, 891–913.
- (31) Bren, U.; Martinek, V.; Florian, J. Decomposition of the solvation free energies of deoxyribonucleoside triphosphates using the free energy perturbation method. *J. Phys. Chem. B* **2006**, *110*, 12782–12788.
- (32) Bren, M.; Florian, J.; Mavri, J.; Bren, U. Do all pieces make a whole? Thiele cumulants and the free energy decomposition. *Theor. Chem. Acc.* **2007**, *117*, 535–540.
- (33) Hamza, A.; Tong, M.; AbdulHameed, M. D. M.; Liu, J.; Goren, A. C.; Tai, H.; Zhan, C. Understanding microscopic binding of human microsomal prostaglandin E synthase-1 (mPGES-1) trimer with substrate PGH<sub>2</sub> and cofactor GSH: Insights from computational alanine scanning and site-directed mutagenesis. *J. Phys. Chem. B* **2010**, *114*, 5605–5616.
- (34) Chavan, S.; Pawar, S.; Singh, R.; Sobhia, M. E. Binding site characterization of G protein-coupled receptor by alanine-scanning mutagenesis using molecular dynamics and binding free energy approach: application to C-C chemokine receptor-2 (CCR2). *Mol. Diversity* **2012**, *16*, 401–413.
- (35) Chiericatti, G.; Santi, D. V. Aspartate 221 of thymidylate synthase is involved in folate cofactor binding and in catalysis. *Biochemistry* **1998**, *37*, 9038–9042.
- (36) Hardy, L. W.; Finer-Moore, J. S.; Montfort, W. R.; Jones, M. O.; Santi, D. V.; Stroud, R. M. Atomic structure of thymidylate synthase: Target for rational drug design. *Science* **1987**, *235*, 448–455.
- (37) Bren, U.; Janežič, D. Individual degrees of freedom and the solvation properties of water. *J. Chem. Phys.* **2012**, *137*, 024108.
- (38) Bren, U.; Krzan, A.; Mavri, J. Microwave catalysis through rotationally hot reactive species. *J. Phys. Chem. A* **2008**, *112*, 166–171.
- (39) Aqvist, J.; Medina, C.; Samuelsson, J. E. A new method for predicting binding affinity in computer-aided drug design. *Protein Eng.* **1994**, *7*, 385–391.
- (40) Bren, U.; Oostenbrink, C. Cytochrome P450 3A4 inhibition by ketoconazole: Tackling the problem of ligand cooperativity using molecular dynamics simulations and free-energy calculations. *J. Chem. Inf. Model.* **2012**, *52*, 1573–1582.
- (41) Lee, F. S.; Chu, Z. T.; Bolger, M. B.; Warshel, A. Calculations of antibody-antigen interactions: microscopic and semi-microscopic evaluation of the free energies of binding of phosphorylcholine analogs to McPC603. *Protein Eng.* **1992**, *5*, 215–228.
- (42) Bren, U.; Lah, J.; Bren, M.; Martinek, V.; Florian, J. DNA duplex stability: The role of preorganized electrostatics. *J. Phys. Chem. B* **2010**, *114*, 2876–2885.